Lithium-Ion Batteries

Deutsche Ausgabe: DOI: 10.1002/ange.201503487
Internationale Ausgabe: DOI: 10.1002/anie.201503487

Hydrothermal Synthesis of Unique Hollow Hexagonal Prismatic Pencils of $Co_3V_2O_8{\cdot}nH_2O$: A New Anode Material for Lithium-Ion Batteries**

Fangfang Wu, Shenglin Xiong, Yitai Qian, and Shu-Hong Yu**

Abstract: *Hollow structures of transition-metal oxides, particularly mixed-metal oxides, could be promising for various applications such as lithium-ion batteries (LIBs). Compared to the synthesis of metal oxide hollow spheres by the template method, non-spherical metal oxide hollow hexagonal polyhedra have not been developed to date. Herein, we report the controlled hydrothermal synthesis of a new phase of $Co_3V_2O_8{\cdot}nH_2O$ hollow hexagonal prismatic pencils (HHPPs), which is composed of uniform structural units. By varying the amount of NaOH in the presence of NH_4^+ and without any template or organic surfactant, the hexagonal prismatic pencils gradually transform from solid into hollow structures, with sizes varying from 5 to 20 μm. The structure of pencils can be preserved only in a limited range of the molar ratio of OH^-/NH_4^+. As a new anode material for LIBs, such hollow pencils exhibit impressive lithium storage properties with high capacity, good cycling stability, and superior rate capability.*

Hollow micro-/nanostructures have attracted considerable attention because of their structure-dependent properties and widespread applications in many areas, including catalysis, drug delivery, biomedicine, and energy storage and conversion.[1–4] As a result, the controllable preparation of hollow materials with a complex composition and delicate morphological control has become increasingly fascinating and vital for both fundamental studies and practical applications. A variety of synthetic protocols have been developed to prepare various hollow structures with different morphologies and desired micro- and nanostructures based on different principles, including the Kirkendall effect, galvanic replacement, ionic exchange, chemical etching, and templating and Ostwald ripening.[5–10] To date, most complex hollow structures have been synthesized through templating strategies using different colloidal templates, and the geometry of these products obtained in practice is mostly spherical. For example, Xu and Wang prepared multishelled Cu_2O hollow spheres by a multilamellar micelle templating route.[7] Lai et al. designed a general route for the synthesis of several oxide multi-shelled hollow microspheres using carbonaceous microspheres as templates, which manifest improved gas-sensing properties.[9] Zeng and Xiong reported the synthesis of multishelled Cu_2S hollow spheres by a serial ion-exchange method.[10] Nevertheless, there have been no reports to date on the formation of non-spherical hollow structures with complex geometry solely by in situ selective inhibition of growth in certain planes.

Mixed-valence metal oxides with different metal cations have demonstrated high electrochemical activities due to their interfacial effects and the synergic effects of the multiple metal species.[11–13] Nevertheless, in contrast to the active research on the synthesis of mixed transition-metal oxides (TMOs; donated as $A_xB_{3-x}O_4$; A, B = Co, Ni, Zn, Mn, Fe)[11] as important mixed-metal oxides, metal vanadates appear to be underexplored, likely because of the lack of suitable synthetic methods.[14–16]

Herein, we report the hydrothermal synthesis of the new phase of $Co_3V_2O_8{\cdot}nH_2O$ with non-spherical structures and a complex geometry. With properly manipulating the precursor system and thus reaction kinetics, the growth of certain specific planes could be inhibited simply by changing the NaOH content in the presence of NH_4^+ without the use of any template or surfactant; this approach resulted in the gradual evolution of solid hexagonal prismatic pencils into concave hexagonal prismatic pencils and finally into hollow hexagonal prismatic pencils (HHPPs). As shown in Figure 1, we used cobalt salt and ammonium metavanadate as reaction precursors by varying the amount of NaOH to establish general principles for controlling/inhibiting the growth of some planes and the hollowing process for the synthesis of $Co_3V_2O_8{\cdot}nH_2O$ pencils. Impressively, when applied as an anode material for LIBs, these $Co_3V_2O_8{\cdot}nH_2O$ HHPPs exhibit a high specific capacity with an excellent rate capability and enhanced cycling stability, making them potential electrode materials for LIBs.

[*] Dr. F. F. Wu, Prof. S. L. Xiong, Prof. Y. T. Qian
Key Laboratory for Colloid and Interface
Ministry of Education and
School of Chemistry and Chemical Engineering
Shandong University, Jinan, 250100 (P.R. China)
E-mail: chexsl@sdu.edu.cn
Prof. Y. T. Qian, Prof. S. H. Yu
Division of Nanomaterials and Chemistry
Hefei National Laboratory for Physical Sciences at Microscale
Collaborative Innovation Center of Suzhou Nano Science and Technology, Department of Chemistry
University of Science and Technology of China
Hefei, Anhui 230026 (P.R. China)
E-mail: shyu@ustc.edu.cn
Homepage: http://staff.ustc.edu.cn/≈yulab/

[**] This work was supported by the National Basic Research Program of China (grant numbers 2011CB935901, 2014CB931800, and 2013CB933900), National Natural Science Fund of China (grant numbers 21371108, 21431006, and 91227103), and Shandong Provincial Natural Science Foundation for Distinguished Young Scholar (grant number JQ201304).

Supporting information for this article is available on the WWW under http://dx.doi.org/10.1002/anie.201503487.

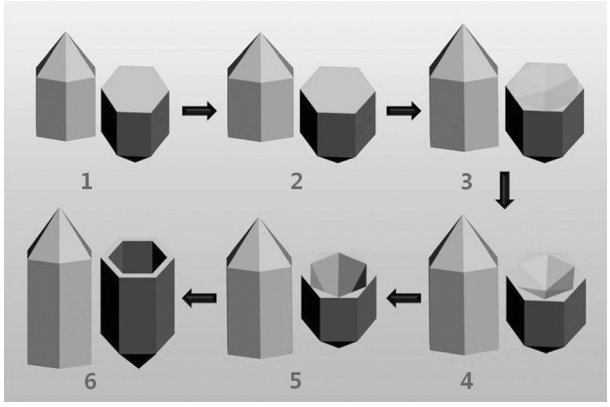

Figure 1. Formation of the new phase of $Co_3V_2O_8{\cdot}n\,H_2O$ HHPPs synthesized herein. The sequence proceeds from solid hexagonal prismatic pencils (including 1 and 2) gradually transforming into concave structures (including 3, 4, and 5), and finally into HHPPs (6).

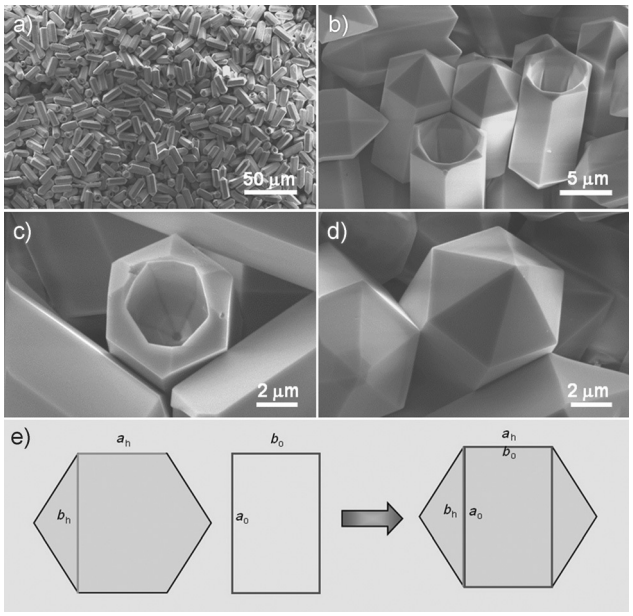

Figure 2. Structural and morphological study of $Co_3V_2O_8{\cdot}n\,H_2O$ HHPPs obtained at NH_4VO_3/NaOH = 2:2 at 200 °C over 48 h: a–d) representative FESEM images. e) A projected crystal unit cell without the types of ions along the $[001]_o$ axis of the orthorhombic $Co_3V_2O_8{\cdot}n\,H_2O$ structure.

The as-prepared cobalt–vanadium oxide was confirmed as a new phase of $Co_3V_2O_8{\cdot}H_2O$ based on combined structural analyses. To this end, the chemical composition and status of the sample was characterized by various techniques. As shown in the X-ray photoelectron spectroscopy (XPS) survey spectra (see Figure S1 in the Supporting Information), cobalt, vanadium, and oxygen, as well as carbon from the reference, could be detected without any other impurities. The two Co $2p_{3/2}$ and Co $2p_{1/2}$ peaks located at 780.8 and 796.7 eV in the Co 2p spectrum of Figure S1 b are accompanied by two shake-up satellite peaks (786.3 and 802.8 eV), which are characteristic of Co^{II}.[17] The V 2p spectrum (Figure S1 c) confirmed that the binding energies for V $2p_{3/2}$ and V $2p_{1/2}$ are consistent with the literature values for V^{5+}.[18] With respect to the O1 s orbital spectrum, a strong peak at approximately 530.1 eV is assigned to oxygen in the metal–oxygen bonds (Figure S1 d).[18] Moreover, combined energy-dispersive X-ray spectroscopy (EDX) and combined inductive coupled plasma atomic emission spectrometer (ICP-AES) analyses further determined the molar ratios of Co:V to be 3:2 (Table S1 and Figure S2).

The corresponding X-ray powder diffraction (XRD) pattern provides further verification of the detailed structural and phase information used to index the as-obtained cobalt–vanadium oxide as a new phase of $Co_3V_2O_8{\cdot}n\,H_2O$. XRD pattern in Figure S3a cannot be assigned to any Co- or V-included materials reported previously, suggesting the appearance of a new type of material. Thorough investigation reveals that the material has a diffraction pattern similar to that of $Co_3As_2O_8{\cdot}n\,H_2O$ (JCPDF 32-0291). Based on the corresponding indexing referred to JCPDF 32-0291, cell parameters of $Co_3V_2O_8{\cdot}n\,H_2O$ are calculated to be $a =$ 11.2000 Å, $b = 6.4860$ Å, and $c = 5.0840$ Å (see section S3 in the Supporting Information). In other words, the as-fabricated cobalt–vanadium oxide can be reasonably concluded to be a new phase of $Co_3V_2O_8{\cdot}n\,H_2O$ with an orthorhombic system that is isostructural with the known $Co_3As_2O_8{\cdot}n\,H_2O$.

A low-magnification field-emission scanning electron microscopy (FESEM) image (Figure 2 a) panoramically indicates that the synthesized samples consisted of HHPPs with a narrow size distribution. It can be observed from Figure 2 b–d that the particle shape resembles that of common pencils with hexagonal hollow prismatic stems and pyramidal tips. The outside surface is very smooth. The featured pencils possess an average diameter of about 6.0 μm and a length of about 25 μm. The $Co_3V_2O_8{\cdot}n\,H_2O$ pencils appear to have "perfectly" symmetrical hexagonal stems, which is supposed to be the intrinsic nature of higher-symmetry systems, suggesting a contradiction. From a crystallographic standpoint, certain single-crystal structures of low-symmetry systems can take on the pseudo-high symmetry of higher-class cubic or hexagonal phases because the cell parameters of the former are coincidentally close to the crystallographic relationship of the latter. Figure 2 e shows the illustrated projected unit cells of the orthorhombic and hexagonal phases along $[001]_o$ and $[0001]_h$. Based on the hexagonal symmetry, b_h must be equal to $\sqrt{3}a_h$, that is, $b_{h=}\sqrt{3}a_h = 1.7320a_h$. In this instance, as for $Co_3V_2O_8{\cdot}n\,H_2O$ (calculated above), we can obtain the crystallographic axis relation as follows: $a_o = 1.7268\,b_o$. The orthorhombic phase of $Co_3V_2O_8{\cdot}n\,H_2O$ transforms because of the lattice distortion of the hexagonal system, due to certain internal strain factors resulting from oxygen vacancies or crystalline defects introduced during preparation.[19,20] Further materials characterization with high-resolution TEM and EDX mappings can be found in Figure S4.

In the formation of HHPPs, the amount of NaOH plays a crucial role in the formation and morphological control of the final product when the NH_4^+ concentration was fixed (also see Figures S5–S11). The average diameter of solid hexagonal pencils (defined as the diagonal distance of hexagonal plate) evolved to 4 μm in diameter and 5.5 μm in

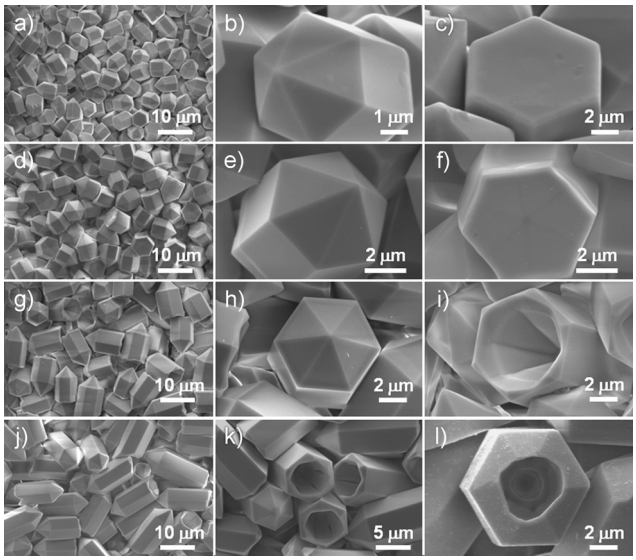

Figure 3. Structural and morphological evolution of $Co_3V_2O_8{\cdot}n\,H_2O$ hexagonal prismatic pencils visualized by FESEM at 200 °C for 14 h with different molar ratios of NH_4VO_3 to NaOH: a–c) 2:1, d–f) 2:1.25, g–i) 2:1.5, and j–l) 2:1.75.

length at 1.0 mmol NaOH (1.25×10^{-2} M, pH 8.6; Figure 3 a–c). The bottom of the structures took on the shape of a concave polyhedral as the NaOH concentration was increased to 1.25 mmol (3.125×10^{-2} M, pH 8.7; Figure 3 d–f). By comparing the results presented in Figure 2 with those discussed above, the higher concentration of NaOH contributed to the formation of hollow structures. As expected, the concave pencils gradually became hollow as the concentration of NaOH was increased from 1.5 and 1.75 up to 2.0 mmol, wherein the pH of the solution corresponded to 8.9 and 9.0 to 9.3, respectively (Figure 3 g–l). By comparison with the above results, the higher basicity resulted in the overall size increase of the pencil crystals by more than 25-fold in length from 1 μm to more than 25 μm and only 1.5-fold in diameter from 4 to about 6 μm, confirming that the growth rate in the longitudinal direction was higher than that along the transverse direction. A similar phenomenon was reported for Ag prisms controlled by different structure-directed agents.[21–23] In our system, $Co_3V_2O_8{\cdot}n\,H_2O$ pencils could not overgrow and become hollow using the well-grown solid $Co_3V_2O_8{\cdot}n\,H_2O$ pencils as starting seeds even though an appropriate amount of NaOH was involved (Figure S12). Hence, the hollowing process is not due to the etching caused by the alkaline medium, in contrast to the previous reported results.[24] All diffraction peaks of XRD of types of pencils are consistent with Figure S3 (Figure S13).

To investigate the formation process of pencils, NH_4VO_3 was replaced by another vanadium source, $NaVO_3$. For comparison, the pH value of solution was adjusted to be 8.5 and 9.0 by adding 0.25 and 0.75 mmol NaOH, respectively, similar to that in the NH_4VO_3 system described above with the addition of 1.0–1.75 mmol NaOH. Nevertheless, the pencils could not be obtained under either set of conditions (Figure S14). However, if other NH_4^+-containing reagents were used, such as NH_4Cl, NH_4F, $(NH_4)_2SO_4$ or even $CO(NH_2)_2$, in the presence of $NaVO_3$, surprisingly, pencils could also be synthesized (Figures S15–16). On the other hand, under the same respective conditions, when other inorganic bases, namely KOH, LiOH and Na_2CO_3, were substituted for NaOH, we also obtained pencil-like structures (Figure S17). Moreover, when other cobalt salts such as $Co(NO_3)_2$, $CoSO_4$, or $Co(CH_3COO)_2$ were substituted for $CoCl_2$, pencils could also be achieved (Figure S18). Some studies have verified the effect of inorganic ions on the structural evolution or kinetics of the final crystals produced.[25,26] By applying different ion species, particles can be engineered into nanowires or into nanoplates, whereas in our system, a variety of anions, including Cl^-, F^-, SO_4^{2-} and CO_3^{2-}, as well as cations, including Na^+, K^+, and Li^+, did not exert a modulatory effect on the morphological development of the final structures. Based on these discussions, NH_4^+ ions played a pivotal role in the formation of pencil-like shaped polyhedra within a certain basicity range.

The results of the detailed analyses conducted in this study can be explained as follows. First, NH_4^+ and the derived $NH_3{\cdot}H_2O$ formed a buffer solution, which stabilized the basic environment. Second, NH_3 derived from NH_4^+ could react with $[Co(H_2O)_6]^{2+}$ to produce the more stable $[Co(NH_3)_6]^{2+}$. With an increase in the concentration of OH^-, the reaction equilibrium was destroyed and moved toward favoring the formation of $[Co(NH_3)_6]^{2+}$. Herein, by regulating the slow release of free Co^{2+} from $[Co(NH_3)_6]^{2+}$, the rate of homogeneous nucleation, the first stage of the crystallization process, was well-controlled, resulting in the generation of fewer nuclei and thus final crystals of a larger size. Slow mass transport improved the rate of the controlled growth stage, which was favorable for the anisotropic development of the crystals. In the present system, no other foreign active sites were supplied for $Co_3V_2O_8{\cdot}n\,H_2O$ nucleation, unlike in heterogeneous nucleation. Thus, the crystallization behavior dominated the resulting crystalline particle morphology. For the $Co_3V_2O_8{\cdot}n\,H_2O$ low-symmetry system, anisotropic growth along the *c* axis was not induced by its intrinsic properties. Different types of quaternary ammonium, such as CTAB and CTAC, can impart functionality and versatility to inorganic crystals by binding to certain facets of nuclei.[27] Thus, nuclei are stabilized against aggregation by a repulsive force, which, in general, dominates the formation of crystals in terms of the growth rate of certain facets, ultimate size, and geometric configuration. With fewer OH^- ions applied, {001} facets could be retained, which disappeared under reverse condition. More NH_4^+ cations were bound to {001} planes and were stabilized in the final crystals. Lower concentrations were not sufficient to deactivate the {001} facets. Because of the loss of adsorption by NH_4^+, hexagonal prismatic polyhedra prefer to grow along the (001) direction, thus making {001} planes disappear and inducing faster vertical growth. As a consequence, NH_4^+ can be reasonably concluded to be bound more strongly to {001} planes, resulting in its presence in the final product. As reported previously, PVP and citrate capping agents likewise show similar preferential adsorption on {111} facets of face-centered cubic crystals and contribute to the formation of different facet-dominated nanocrystals.[21] Accompanying the disappearance of {100} facets, {*3–1l*},

{*31l*} and {*04l*} crystal facets grew to constitute the inner lateral faces of the hollow structures. Upon continuously increasing the concentration of OH^- ions (less NH_4^+ ions), the *l* values became larger, corresponding to the larger hollow depth of the $Co_3V_2O_8{\cdot}n\,H_2O$ HHPPs.

Our time-dependent experiments indeed are consistent with the above mechanism (Figures S19 and S20). Under the current synthetic conditions, the rate of vertical growth was much higher than that of lateral growth, thus increasing the ratio of length to diameter as the reaction proceeded (Figure S19). The effect of reaction temperature on the formation of well-defined pencils was also explored. Higher temperature was observed to favor the thermal decomposition of metavanadate and ensured a sufficient supply of pentavalent vanadium ions and the formation of pencils (Figure S21). The order of addition of the cobalt salts and OH-ions did not change the final morphology of products (Figure S22). Thus, the proposed synthesis procedure provides a general means for controlling the product morphology.

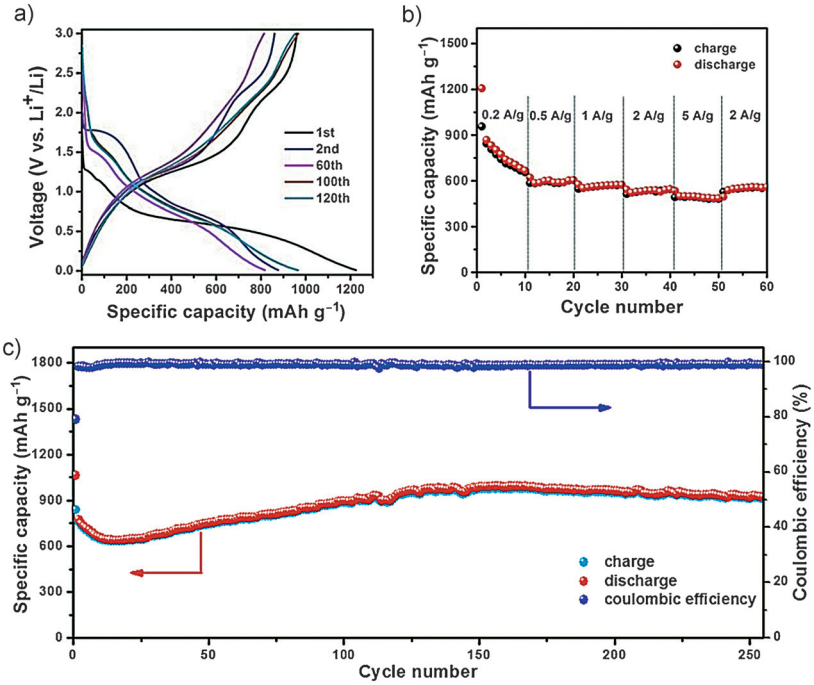

Figure 4. Electrochemical performance of a $Co_3V_2O_8{\cdot}n\,H_2O$ HHPPs electrode. a) Discharge–charge curves in the voltage of 0.01–3 V; b) rate performance at different current densities; c) cycling performance and corresponding CE at a current of 0.5 $A\,g^{-1}$.

The electrochemical performance of the $Co_3V_2O_8{\cdot}n\,H_2O$ HHPPs is examined as an anode material for lithium-ion batteries (LIBs). Figure S23 shows the cyclic voltammogram (CV) curves of the first five cycle curves of the electrode at a scan rate of 0.1 $mV\,s^{-1}$. In the first cathodic scan, the two cathodic peaks observed at voltage potentials of 1.31 and 0.44 V can be assigned to the transformation of $Co_3V_2O_8{\cdot}n\,H_2O$ into CoO accompanied by the formation of $Li_xV_2O_5$ and the reduction of Co^{2+} to Co^0, respectively, which is in agreement with results reported in the literature.[15,28] From the second cycle onwards, the CV curves are mostly overlapped, which shows the good reversibility of the electrochemical reactions (Figure S23).

The representative charge/discharge curves of the 1st, 2nd, 60th, 100th, and 120th cycles for the $Co_3V_2O_8{\cdot}n\,H_2O$ electrode at a current density of 0.2 $A\,g^{-1}$ are shown in Figure 4a. The initial discharge and charge specific capacities are 1224 and 960 $mAh\,g^{-1}$, respectively, and offer an ideal initial Coulombic efficiency (CE) of 78%. The discharge capacity falls to 815 $mAh\,g^{-1}$ at the 60th cycle and then gradually rises to 953 $mAh\,g^{-1}$ at the 120th cycle, at which point the discharge capacity tends to stabilize. The rate capability of $Co_3V_2O_8{\cdot}n\,H_2O$ was investigated by gradually increasing the current density from 0.2 to 5 $A\,g^{-1}$ and then returning it to 2 $A\,g^{-1}$ (Figure 4b). The average discharge capacities of the $Co_3V_2O_8{\cdot}n\,H_2O$ were 800, 596, 566, 534, and 496 $mAh\,g^{-1}$ at the current densities of 0.2, 0.5, 1, 2, and 5 $A\,g^{-1}$, respectively. Even after the current density was returned to 2 $A\,g^{-1}$, a discharge capacity of over 500 $mAh\,g^{-1}$ could be recovered. The capacity could be retained to be as high as 502 $mAh\,g^{-1}$ even after 270 cycles without any losses, and the CE reached nearly 99% (Figure S24). Furthermore, the $Co_3V_2O_8{\cdot}n\,H_2O$ HHPP electrode possesses remarkable cyclic stability (Figure 4c). The initial discharge- and charge-specific capacities are 1063 and 839 $mAh\,g^{-1}$, respectively, corresponding to the higher initial CE of 78.9%. It is interesting to observe that the discharge capacity decreases slightly before the 25th cycle. Beyond that point, there is a slight increase in the discharge capacity until the 150th cycle, which then remains stable for more than 255 cycles. First, the deconstruction of the crystal $Co_3V_2O_8{\cdot}n\,H_2O$ in the conversion reactions could reduce the conductivity of the electrode in the first discharge process, which could synergistically affect the lithium storage and lead to capacity fading at an early stage. After charging and discharging at a low current, the electrolyte can gradually penetrate into the inner part of the active materials. After 255 cycles, a discharge capacity of 847 $mAh\,g^{-1}$ can be retained, with a corresponding CE greater than 98%, indicating excellent cycling stability. These results suggest that the structure of $Co_3V_2O_8{\cdot}n\,H_2O$ is stable even under high-rate, long-cycling conditions, which is important for practical applications. After cycling, the initial structure can be well retained (Figure S25). The improved electrochemical activities are mostly attributed to the unique architectural structures, which feature accessible active sites over the entire surface. Furthermore, the improved electrochemical activity is related to the possible synergetic effects of different metal ions.

In summary, we demonstrated, for the first time, a facile hydrothermal approach for the controlled synthesis of a unique new phase of $Co_3V_2O_8{\cdot}n\,H_2O$ hollow hexagonal prismatic pencils (HHPPs) without using any templates or surfactants. Introducing different amounts of NaOH into the

reaction system allowed for the size-controlled synthesis of such HHPPS with sizes ranging from 5 to 20 μm. The OH^-/NH_4^+ ratio was found to play crucial roles in the formation of $Co_3V_2O_8{\cdot}nH_2O$ HHPPs. Because of the unique architectures and the synergistic effect of different metal ions, these unique new phase of $Co_3V_2O_8{\cdot}nH_2O$ HHPPs exhibit superior electrochemical performance as anode materials for LIBs. This work provides not only a versatile approach to the synthesis of uniform non-spherical hollow nanoarchitectures in contrast to spherical hollow structures, but also a new material for lithium-ion batteries.

Keywords: electrochemistry · catalysis · lithium-ion batteries · mixed-metal oxides · nanostructures

How to cite: *Angew. Chem. Int. Ed.* **2015**, *54*, 10787–10791
Angew. Chem. **2015**, *127*, 10937–10941

[1] X. W. Lou, L. A. Archer, Z. C. Yang, *Adv. Mater.* **2008**, *20*, 3987.
[2] J. H. Sun, J. S. Zhang, M. W. Zhang, M. Antonietti, X. Z. Fu, X. C. Wang, *Nat. Commun.* **2012**, *3*, 1139.
[3] Z. W. Seh, W. Y. Li, J. J. Cha, G. Y. Zheng, Y. Yang, M. T. McDowell, P. C. Hsu, Y. Cui, *Nat. Commun.* **2013**, *4*, 1331.
[4] Z. Y. Wang, L. Zhou, X. W. Lou, *Adv. Mater.* **2012**, *24*, 1903.
[5] Y. D. Yin, R. M. Rioux, C. K. Erdonmez, S. Hughes, G. A. Somorjai, A. P. Alivisatos, *Science* **2004**, *304*, 711.
[6] X. W. Lou, C. L. Yuan, Q. Zhang, L. A. Archer, *Angew. Chem. Int. Ed.* **2006**, *45*, 3825; *Angew. Chem.* **2006**, *118*, 3909.
[7] H. L. Xu, W. Z. Wang, *Angew. Chem. Int. Ed.* **2007**, *46*, 1489; *Angew. Chem.* **2007**, *119*, 1511.
[8] C. H. Kuo, M. H. Huang, *J. Am. Chem. Soc.* **2008**, *130*, 12815.
[9] X. Y. Lai, J. Li, B. A. Korgel, Z. H. Dong, M. Z. Li, F. B. Su, J. Du, D. Wang, *Angew. Chem. Int. Ed.* **2011**, *50*, 2738; *Angew. Chem.* **2011**, *123*, 2790.
[10] S. L. Xiong, H. C. Zeng, *Angew. Chem. Int. Ed.* **2012**, *51*, 949; *Angew. Chem.* **2012**, *124*, 973.
[11] C. Z. Yuan, H. B. Wu, Y. Xie, X. W. Lou, *Angew. Chem. Int. Ed.* **2014**, *53*, 1488; *Angew. Chem.* **2014**, *126*, 1512.
[12] F. Y. Cheng, J. A. Shen, B. Peng, Y. D. Pan, Z. L. Tao, J. Chen, *Nat. Chem.* **2011**, *3*, 79.
[13] H. Q. Li, X. Z. Liu, T. Y. Zhai, D. Li, H. S. Zhou, *Adv. Energy Mater.* **2013**, *3*, 428.
[14] H. Ma, S. Y. Zhang, W. Q. Ji, Z. L. Tao, J. Chen, *J. Am. Chem. Soc.* **2008**, *130*, 5361.
[15] G. Z. Yang, H. Cui, G. W. Yang, C. X. Wang, *ACS Nano* **2014**, *8*, 4474.
[16] M. Xing, L. B. Kong, M. C. Liu, L. Y. Liu, L. Kang, Y. C. Luo, *J. Mater. Chem. A* **2014**, *2*, 18435.
[17] S. A. Needham, G. X. Wang, K. Konstantinov, Y. Tournayre, Z. Lao, H. K. Liu, *Electrochem. Solid-State Lett.* **2006**, *9*, A315.
[18] D. L. Chao, X. H. Xia, J. L. Liu, Z. X. Fan, C. F. Ng, J. Y. Lin, H. Zhang, Z. X. Shen, H. J. Fan, *Adv. Mater.* **2014**, *26*, 5794.
[19] K. Y. Yun, D. Ricinschi, T. Kanashima, M. Noda, M. Okuyama, *Jpn. J. Appl. Phys.* **2004**, *43*, L647.
[20] K. Y. Yun, M. Noda, M. Okuyama, H. Saeki, H. Tabata, K. Saito, *J. Appl. Phys.* **2004**, *96*, 3399.
[21] J. Zeng, X. H. Xia, M. Rycenga, P. Henneghan, Q. Li, Y. N. Xia, *Angew. Chem. Int. Ed.* **2011**, *50*, 244; *Angew. Chem.* **2011**, *123*, 258.
[22] S. L. Xiong, B. J. Xi, K. Zhang, Y. F. Chen, J. W. Jiang, J. Y. Hu, H. C. Zeng, *Sci. Rep.* **2013**, *3*, 2177.
[23] J. Zeng, Y. Q. Zheng, M. Rycenga, J. Tao, Z. Y. Li, Q. Zhang, Y. M. Zhu, Y. N. Xia, *J. Am. Chem. Soc.* **2010**, *132*, 8552.
[24] Z. Y. Wang, Z. C. Wang, H. B. Wu, X. W. Lou, *Sci. Rep.* **2013**, *3*, 1391.
[25] Z. S. Hu, G. Oskam, R. L. Penn, N. Pesika, P. C. Searson, *J. Phys. Chem. B* **2003**, *107*, 3124.
[26] G. Oskam, Z. Hu, R. L. Penn, N. Pesika, P. C. Searson, *Phys. Rev. E* **2002**, *66*, 011403.
[27] Y. Y. Ma, W. Y. Li, E. C. Cho, Z. Y. Li, T. Y, J. Zeng, Z. X. Xie, Y. N. Xia, *ACS Nano* **2010**, *4*, 6725.
[28] L. Zhou, D. Zhao, X. W. Lou, *Adv. Mater.* **2012**, *24*, 745.

Received: April 16, 2015
Published online: July 23, 2015

